Journal of Physics: Conference Series **2156** (2022) 012227 doi:10.1088/1742-6596/2156/1/012227

Cosmic activation of CRESST's $CaWO_4$ crystals

H Kluck[1], G Angloher[2], G Benato[3], A Bento[2,9], A Bertolini[2], R Breier[4], C Bucci[3], L Canonica[2], A D'Addabbo[3], S Di Lorenzo[3], L Einfalt[1,5], A Erb[6,11], F v. Feilitzsch[6], N Ferreiro Iachellini[2], S Fichtinger[1], D Fuchs[2], A Fuss[1,5], A Garai[2], V M Ghete[1], P Gorla[3], S Gupta[1], D Hauff[2], M Ješkovský[4], J Jochum[7], M Kaznacheeva[6], A Kinast[6], H Kraus[8], A Langenkämper[6], M Mancuso[2], L Marini[3], V Mokina[1], A Nilima[2], M Olmi[3], T Ortmann[6], C Pagliarone[3,12], V Palušová[4], L Pattavina[6,10], F Petricca[2], W Potzel[6], P Povinec[4], F Pröbst[2], F Pucci[2], F Reindl[1,5], J Rothe[6], K Schäffner[2], J Schieck[1,5], D Schmiedmayer[1,5], S Schönert[6], C Schwertner[1,5], M Stahlberg[2], L Stodolsky[2], C Strandhagen[7] R Strauss[6], I Usherov[7], F Wagner[1], M Willers[6] and V Zema[2]
(CRESST Collaboration)

[1] Institut für Hochenergiephysik der Österreichischen Akademie der Wissenschaften, A-1050 Wien, Austria
[2] Max-Planck-Institut für Physik, D-80805 München, Germany
[3] INFN, Laboratori Nazionali del Gran Sasso, I-67100 Assergi, Italy
[4] Comenius University, Faculty of Mathematics, Physics and Informatics, 84248 Bratislava, Slovakia
[5] Atominstitut, Technische Universität Wien, A-1020 Wien, Austria
[6] Physik-Department and Excellence Cluster Universe, Technische Universität München, D-85747 Garching, Germany
[7] Eberhard-Karls-Universität Tübingen, D-72076 Tübingen, Germany
[8] Department of Physics, University of Oxford, Oxford OX1 3RH, United Kingdom
[9] also at: Departamento de Fisica, Universidade de Coimbra, P3004 516 Coimbra, Portugal
[10] Also at: GSSI-Gran Sasso Science Institute, I-67100 L'Aquila, Italy
[11] Also at: Walther-Meißner-Institut für Tieftemperaturforschung, D-85748 Garching, Germany
[12] Also at: Dipartimento di Ingegneria Civile e Meccanica, Universitá degli Studi di Cassino e del Lazio Meridionale, I-03043 Cassino, Italy

E-mail: holger.kluck@oeaw.ac.at

Abstract. The CRESST experiment searches for dark matter induced nuclear recoils inside $CaWO_4$ based cryogenic calorimeters at the Laboratori Nazionali del Gran Sasso (LNGS) in Italy. To identify reliably a potential signal, a precise understanding of its background budget is crucial. An important background category could be "cosmogenics": radionuclides produced via interactions with cosmic rays, mainly during the crystal production at surface facilities. Albeit $CaWO_4$ is a well-established calorimetric material, no systematic study of its susceptibility for cosmic activation existed so far. In this contribution, we will first report the exposure profile of CRESST's in-house grown TUM93 crystal to cosmic rays. Then we will identify the most prominent cosmogenics via ACTIVIA calculations. Afterwards we discuss the expected background spectrum based on Geant4 simulations and compare it to measurements.

1. Introduction

The nature of Dark Matter (DM) is one of the greatest mysteries in modern physics. The CRESST experiment searches for DM induced nuclear recoils inside $CaWO_4$ monocrystals which are operating as cryogenic calorimeters at $\mathcal{O}(10\,\mathrm{mK})$. By simultaneously measuring the phonon signal and scintillation light emission, electromagnetic background can be rejected. With a nuclear recoil threshold as low as 30.1 eV, CRESST is a world leading DM search for masses $< 2\,\mathrm{GeV}/c$. However, at this energy scale the background rejection capability starts to degrade [1]. Hence, a reliable and complete understanding of the background budget is necessary.

One source of background is the decay of radionuclides that are produced by secondary cosmic rays, so-called *cosmogenics*, inside the $CaWO_4$ crystals. Albeit the production is studied for a vast range of target materials (see e.g. [2] and references therein), so far no systematic study for $CaWO_4$ exist, only case reports e.g. [3, 4, 5]. In this contribution we present first results about the background caused by cosmogenics in a particular $CaWO_4$ crystal: TUM93 with a mass of $m \approx 24\,\mathrm{g}$. It was in-house grown by the CRESST collaboration at the Technische Universität München (TUM). Special care was taken to minimize and log its exposure to cosmic rays.

In section 2, the basic mechanism of cosmic activation is shortly summarized. Afterwards the exposure of TUM93 to cosmic rays is reported in section 3 and in section 4 the production rate of several cosmogenics is calculated. Finally, section 5 concludes with the expected cosmogenic background spectrum for TUM93.

2. Cosmic activation

The production of cosmogenic i is dominated by activation of target x by atmospheric neutrons. Hence, the *production rate* [2]

$$R_{i,x} \propto \int \phi_\mathrm{n}(E)\sigma_{i,x}(E)\mathrm{d}E \tag{1}$$

is proportional to the flux of incident neutrons ϕ_n and the respective cross-section $\sigma_{i,x}$. Values for $CaWO_4$ are given in section 4.

The cosmogenic background activity $A_{i,x}$ depends further on the time of exposure to atmospheric neutrons [2]

$$H_i = \sum_j \left(1 - e^{-\lambda_i \cdot \Delta t_{\mathrm{exp},j}}\right) e^{-\lambda_i \cdot \Delta t_{\mathrm{cool},j}}, \tag{2}$$

which we call the *exposure history* H_i. The first factor describes the *build-up* of i during the time $\Delta t_{\mathrm{exp},j}$ when the target was exposed to atmospheric neutrons, where λ_i is the relevant nuclear decay constant. The second factor describes the subsequent decay of i over the *cool-down* time $\Delta t_{\mathrm{cool},j}$ when the target was shielded. The whole exposure history may be the sum over several individual episodes j of build-up and subsequent cool-down, see figure 1. For TUM93, H_i is reported in section 3.

As $CaWO_4$ is a multi-element target, we weigh the individual targets by their relative molar mass $M_x/M_{\mathrm{CaWO_4}}$:

$$A_i = m \cdot \sum_x \frac{M_x}{M_{\mathrm{CaWO_4}}} R_{i,x} \cdot H_i. \tag{3}$$

where the sum includes all natural isotopes of the target elements ${}_8\mathrm{O}$, ${}_{20}\mathrm{Ca}$ and ${}_{74}\mathrm{W}$.

3. Exposure

Figure 1 illustrates the exposure history of the TUM93 crystal to cosmic rays. Prior to day 182 it was mainly at TUM facilities. When it was not above ground during crystal growth, crystal processing and detector assembly, it was stored at the *Untergrundlabor Garching* (UGL), a

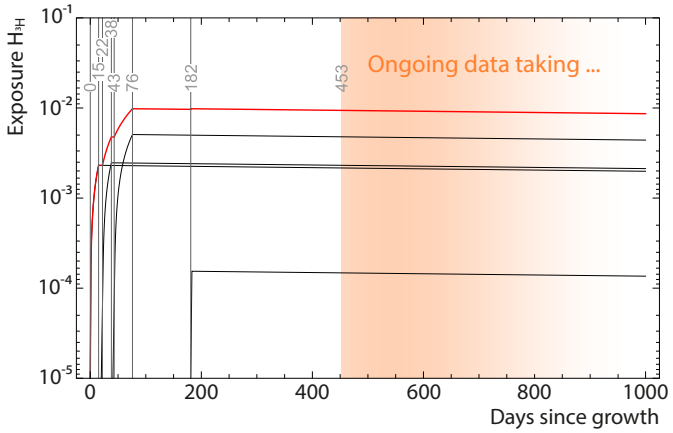

Figure 1. Build-up and cool-down of ^{3}H in the $CaWO_4$ of CRESST's TUM93 crystal. The *black curves* indicate the individual periods of exposure, the *red curve* shows the cumulative exposure $H_{^3H}$. The *orange shaded area* indicates the ongoing data-taking period. The time is given in days since crystal-growth; day 453 corresponds to 1st November 2020. At the time of TAUP2021, the data taking was still ongoing.

Table 1. The ten cosmogenics with the highest production rate R_i in $CaWO_4$, ordered by decreasing R_i.

Nuclide i	^{14}C	^{3}H	^{178}W	^{179}Ta	^{175}Hf	^{181}W	^{37}Ar	^{173}Lu	^{172}Hf	^{171}Lu
R_i / kg^{-1} d^{-1}	84.06	34.82	25.91	24.59	16.67	13.74	12.17	11.25	11.12	9.18

shallow underground laboratory with 15 m w.e. [6] rock overburden. Since day 182, it has been at LNGS (3600 m w.e. [7]). We assume that UGL and LNGS provide perfect shielding against atmospheric neutrons. Future work will evaluate this assumption in case of UGL.

4. Production rates

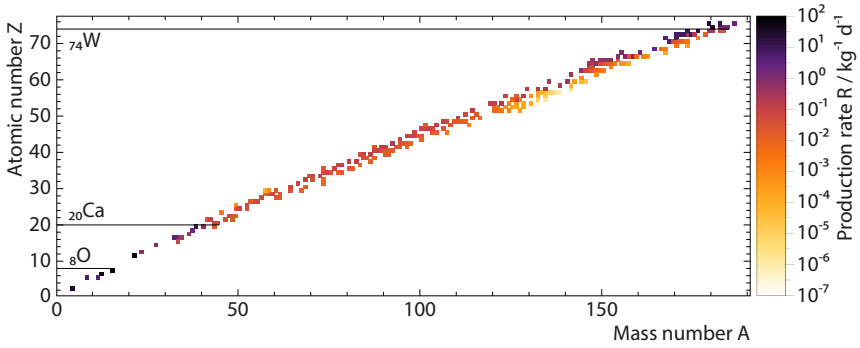

Figure 2. Production rate R_i in the Z-A plane for cosmogenics i produced in a $CaWO_4$ target. Note that due to the binning, the isotopes of the three target elements are *above* the corresponding Z-values.

We used the ACTIVIA code in version 1.3.1 [8] to calculate the production rate R_i of all possible cosmogenics in all natural occurring isotopes of the target elements $_8$O, $_{20}$Ca and $_{74}$W. As shown in figure 2, especially $_{74}$W provides a wide variety of cosmogenics, albeit most of them with strongly supressed production rates.

Concerning the ACTIVIA settings, we used the MENDL-2P data set below 200 MeV for $\sigma_{i,x}$ and ACTIVIA's default parameterisation for the neutron flux ϕ_n. In future work, we will study the robustness of R_i against different data sets and parameterisations.

For the stated conditions, the ten radionuclides with the highest R_i-values are listed in table 1.

5. Cosmogenic background

To predict the background rate B_i caused by the radioactive decay of cosmogenics i in the TUM93 crystal, we integrate equation (3) over the data taking period: $B_i = \int_{t_0}^{t_0+T} A_i \, \mathrm{d}t/(m \cdot T)$.

Table 2. The ten cosmogenics expected to have the highest background rate B_i in TUM93, ordered by decreasing B_i.

Nuclide i	^{179}Ta	^{173}Lu	^{172}Hf	^{3}H	^{181}W	^{175}Hf	^{159}Dy	^{182}Ta	^{143}Pm	^{22}Na
B_i / kg^{-1}d^{-1}	0.96	0.49	0.43	0.32	0.27	0.07	0.05	0.04	0.04	0.02

As the data taking was still ongoing at the time of TAUP2021, we took the actual start time $t_0 = 453\,\mathrm{d}$ but assumed the same period as for the similar detector module used in [1], i.e. $T \approx 240\,\mathrm{d}$. Table 2 lists the cosmogenics with the highest contribution to the background. The difference with respect to table 1 highlights that the exposure not only affects the activity of the most prominent cosmogenics, but also determines which cosmogenics have to be considered at all. Therefore, for different exposure histories, the set of prominent cosmogenics is different.

To obtain the background spectrum, we simulated the decays of the individual cosmogenics with Geant4 version 10.6.3 [9] and scaled them to B_i, see figure 3. Due to their dominant lines, ^{179}Ta ($\approx 11\,\mathrm{keV}$) and ^{181}W ($\approx 17\,\mathrm{keV}$) were already clearly observed in CRESST crystals [3].

The inset of figure 3 compares this background prediction for TUM93 with the previously used TUM40 [4, 5] where the experimentally deduced cosmogenics background was already subdominant. As expected by the even more stringent avoidance of exposure for TUM93, its cosmogenics background should be even more reduced. This confirms the importance of carefully storing the crystals below ground whenever possible.

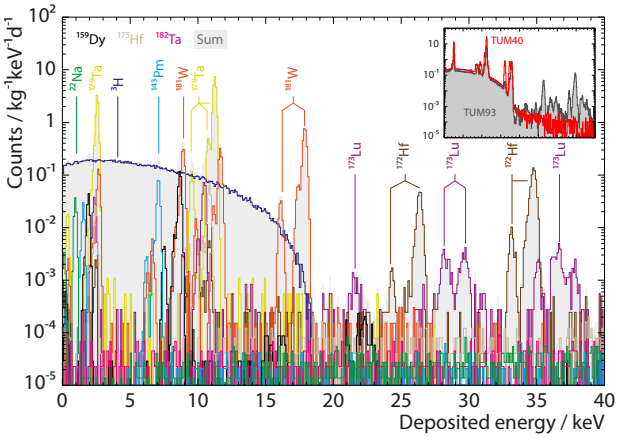

Figure 3. Expected cosmogenic background in TUM93 caused by the ten most prominent cosmogenics. Individual components are given as *colored, unfilled* histograms, the sum is given by the *grey, filled* histogram. The spectrum features characteristic gamma lines, often overlapping e.g. ^{175}Hf, ^{179}Ta and ^{181}W at $\approx 11\,\mathrm{keV}$, and below 18.6 keV the beta-spectrum of ^{3}H. The *inset* shows this sum in *grey* compared to the cosmogenic background in *red* deduced from measurements with TUM40 [4, 5].

Acknowledgments
This work is supported through the DFG by SFB1258 and the Excellence Cluster ORIGINS, and by the BMBF05A17WO4.

References
[1] Abdelhameed A H *et al.* 2019 *Phys. Rev.* D **100** 102002
[2] Cebrián S 2017 *Int. J. Mod. Phys.* A **32** 1743006
[3] Strauss R *et al.* 2015 *J. Cosmol. Astropart. Phys.* **2015** 030
[4] Abdelhameed A H *et al.* 2019 *Eur. Phys. J.* C **79** 881
[5] Abdelhameed A H *et al.* 2019 *Eur. Phys. J.* C **79** 987
[6] Langenkämper A *et al.* 2018 *J. Low Temp. Phys.* **193** 860–866
[7] Ambrosio M *et al.* 1995 *Phys. Rev.* D **52** 3793–3802
[8] Back J J and Ramachers Y A 2008 *Nucl. Instrum. Methods Phys. Res.* A **586** 286–294
[9] Allison J *et al.* 2016 *Nucl. Instrum. Methods Phys. Res.* A **835** 186–225